Quantitative validation of the Boltzmann transport equation phonon thermal conductivity model under the single-mode relaxation time approximation

A. J. H. McGaughey and M. Kaviany*
Department of Mechanical Engineering, University of Michigan, Ann Arbor, Michigan 48109-2125, USA
(Received 22 September 2003; revised manuscript received 15 December 2003; published 16 March 2004)

The phonon thermal conductivity of the Lennard-Jones argon face-centered cubic crystal is predicted between temperatures of 20 K and 80 K using the Boltzmann transport equation under the single-mode relaxation time approximation. The temperature and frequency dependencies of the phonon dispersion and phonon relaxation times are obtained from lattice-dynamics calculations based on the results of molecular-dynamics simulations. No fitting parameters are required. The predicted thermal conductivities are in reasonable agreement with independent predictions made from the simulations using the Green-Kubo method. The assumption of an isotropic medium, as used in the Boltzmann transport equation formulation, leads to an overprediction of the Green-Kubo results at low temperatures. At higher temperatures, where anharmonic effects become increasingly important, the harmonic nature of the relaxation time calculation method leads to an underprediction of the Green-Kubo results. Assuming that the low-frequency behavior of the relaxation times can be extended over the entire frequency range, that there is no dispersion, or that the dispersion is independent of temperature, leads to significant errors in the predictions. This finding indicates that in analytical calculations, where such assumptions are often made, these errors are offset by the use of fitting parameters.

DOI: 10.1103/PhysRevB.69.094303 PACS number(s): 66.70.+f, 63.20.Dj

I. INTRODUCTION

While the lattice dynamics of a harmonic solid can be readily analyzed,[1,2] such a model predicts an infinite phonon thermal conductivity for a perfect crystal (hereafter, the phonon thermal conductivity will be referred to as simply the thermal conductivity). To obtain a finite thermal conductivity, anharmonicities in the atomic interactions, which lead to three-phonon (and higher) processes, must be considered. The inclusion of even three-phonon interactions in the lattice dynamics is a formidable task. A number of techniques for predicting the thermal conductivity based on the Boltzmann transport equation (BTE) have been developed.[1] Notable are those involving the single-mode relaxation time (SMRT) approximation, where every phonon mode is assigned a relaxation time corresponding to the net effect of different scattering mechanisms. A lack of understanding of multiphonon interactions requires that the predictions be fit to the experimental thermal conductivity data. Therefore, while such approaches are useful for qualitatively validating the models developed, the quantitative validity of the models cannot be assessed. As they are currently used, SMRT techniques are thus not suitable for the analysis of materials whose thermal properties are not already known.

The thermal conductivity can also be predicted using the Green-Kubo (GK) method[3] and molecular-dynamics (MD) simulations. In this case, the analysis is based on a statistical-mechanics approach, and is performed in real space [as opposed to the BTE, which is formulated in frequency (phonon) space]. No assumptions about the nature of the thermal transport are required before determining the thermal conductivity. The only required inputs are the equilibrium atomic positions and an appropriate interatomic potential. This approach has generated reasonable agreement with experimental data for a number of dielectric materials.[4–10] The application of MD simulations to real devices is limited by the small system sizes ($\sim$nm) required for reasonable computation times.

The finite size of a MD simulation cell leads to a discrete number of allowed phonon modes, for which relaxation times can be predicted using lattice-dynamic techniques.[11,12] The purpose of this investigation is to use the relaxation times predicted for the Lennard-Jones (LJ) argon face-centered cubic (fcc) crystal to develop a continuous relaxation time function that can then be used in the BTE-SMRT model to predict the thermal conductivity. A summary of this approach to predicting the thermal conductivity, and those described in the preceding two paragraphs, is shown in Fig. 1.

We begin by reviewing the BTE-SMRT and GK thermal conductivity prediction methods. The GK results are presented, and the decomposition of the thermal conductivity into components associated with short and long length scale interactions is described. Methods for predicting the specific heat, anharmonic phonon dispersion, and phonon relaxation times using MD are then presented. A continuous model for the relaxation times is developed, and used with the specific-heat and dispersion data to predict the thermal conductivity with the BTE-SMRT method. To the best of our knowledge, this is the first such calculation performed with no fitting parameters. The GK and BTE-SMRT results are found to agree reasonably well. Common simplifications used in the BTE-SMRT approach are examined, and found to strongly affect the predictions.

II. THERMAL-CONDUCTIVITY PREDICTION

A. Boltzmann transport equation

1. Preliminaries

The BTE for a phonon mode i under a temperature gradient ∇T is given by[1]

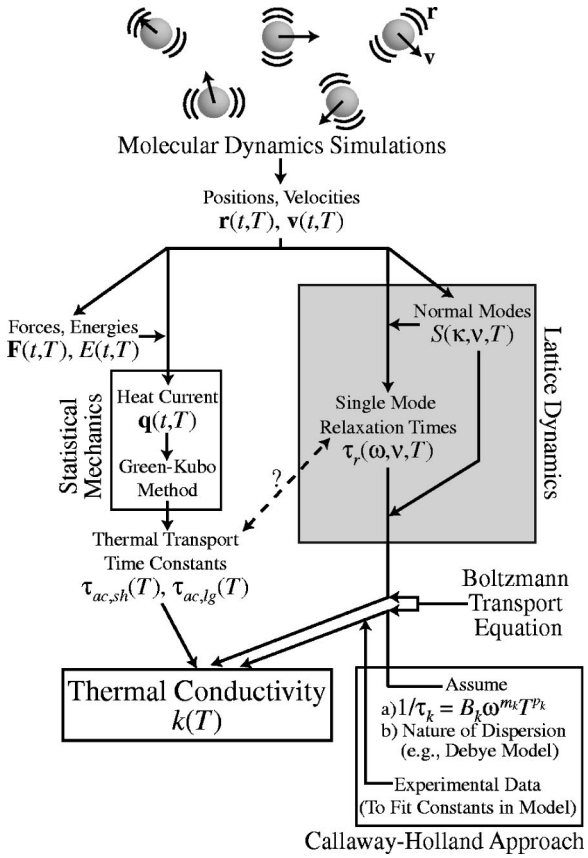

FIG. 1. Flow chart showing different methods by which the thermal conductivity can be predicted. The focus of the current investigation is through the lattice dynamics path.

$$-\mathbf{v}_{g,i}\cdot\nabla T\frac{\partial n_i}{\partial T}+\left(\frac{\partial n_i}{\partial t}\right)_{collision}=0, \tag{1}$$

where n_i is the phonon mode occupation number, t is the time, and $\mathbf{v}_{g,i}$ is the phonon group velocity, defined as $\partial\omega/\partial\boldsymbol{\kappa}$, where ω is the angular frequency and $\boldsymbol{\kappa}$ is the wave vector. The solution of Eq. (1) describes the steady-state distribution of phonons in a system, and how that distribution comes about through the effects of diffusion (first term) and scattering (second term, also known as the collision term).

The main challenge in the solution of Eq. (1) is the modeling of the collision term. Under the SMRT approximation, a relaxation time $\tau_{i,r}$ is assigned to each phonon mode such that[1]

$$\left(\frac{\partial n_i}{\partial t}\right)_{collision}=\frac{n_{i,o}-n_i}{\tau_{i,r}}, \tag{2}$$

where $n_{i,o}$ corresponds to the equilibrium phonon occupation number, given by the Bose-Einstein distribution. The relaxation time describes the temporal response of the system in question when that particular phonon mode is activated. Equation (2) can be used to solve Eq. (1) for n_i. By integrating over all phonon modes, neglecting the contribution of optical phonons, and assuming an isotropic phonon dispersion with degenerate transverse branches, the thermal conductivity k can be expressed using the Fourier law of heat conduction as[13]

$$k=\frac{1}{6\pi^2}\left[\int_0^{\omega_{L,max}}\left(c_v\frac{v_g}{v_p^2}\tau_r\right)_L\omega^2 d\omega+2\int_0^{\omega_{T,max}}\left(c_v\frac{v_g}{v_p^2}\tau_r\right)_T\omega^2 d\omega\right]. \tag{3}$$

Here, L and T correspond to the longitudinal and transverse phonon polarizations, respectively, $\omega_{L,max}$ and $\omega_{T,max}$ are the frequencies of the dispersion branches at the edge of the first Brillouin zone, c_v is the specific heat per mode at constant volume (and thus has units of J/K), and v_p is the phonon phase velocity, defined as ω/κ. All of the quantities inside the integrals are functions of frequency.

2. Callaway-Holland approach

The challenge in the evaluation of the integrals in Eq. (3) is the specification of the phonon relaxation times and how the phonon dispersion (which affects the velocity terms and the upper limits of the integrals) is modeled. Here, an MD simulation cell with periodic boundary conditions and no defects is considered, so that the only source of phonon scattering is through anharmonic interactions between the phonon (normal) modes. There are two types of such interactions: normal (N) processes, which conserve crystal momentum, and Umklapp (U) processes, which do not. An effective relaxation time for each mode $\tau_{i,c}$ is then defined as[14]

$$\frac{1}{\tau_{i,c}}=\frac{1}{\tau_{i,N}}+\frac{1}{\tau_{i,U}}. \tag{4}$$

Note that $\tau_{i,c}$ is not the same as the relaxation time $\tau_{i,r}$ that appears in Eq. (2). This is because the N and U processes have different effects on the phonon distribution, such that in this formulation, the collision term must be modeled as[14]

$$\left(\frac{\partial n_i}{\partial t}\right)_{collision}=\frac{n_{i,\lambda}-n_i}{\tau_{i,N}}+\frac{n_{i,o}-n_i}{\tau_{i,U}}, \tag{5}$$

where $n_{i,\lambda}$ is the distribution that normal processes tend towards. The relationship between $\tau_{i,r}$, $\tau_{i,c}$, $\tau_{i,N}$, and $\tau_{i,U}$ was first established by Callaway.[14]

The $\tau_{i,N}$ and $\tau_{i,U}$ terms are generally modeled with continuous expressions of the form[14,15]

$$\frac{1}{\tau_k}=B_k\omega^{m_k}T^{p_k},\quad k=N,U, \tag{6}$$

where m_k and p_k are integers, and B_k is a constant. The choice of m_k and p_k is often based on theoretical predictions limited to low frequencies (where an elastic medium can be assumed), and/or for convenience in the subsequent calculations. At low temperatures, it has been predicted that the sum of m_k and p_k should be five, and at high temperatures, that p_k should be unity.[1,16] There is no available method for predict-

ing the B_k coefficients, and closure of BTE-SMRT techniques is dependent on the fitting of these parameters with the experimental thermal conductivity data. There is no closed form expression available that covers the entire frequency and temperature ranges of the relaxation times for a given material. As will be shown, an expression of the form of Eq. (6) would not adequate for this purpose.

Callaway[14] modeled germanium using a formulation based on Eq. (5). He assumed a Debye model for the phonon density of states (i.e., no dispersion) did not distinguish between the longitudinal and transverse polarizations, and accounted for the three-phonon interactions using terms with m_k and p_k equal to two and three, respectively [see Eq. (6)]. The resulting expression for the thermal conductivity contained two terms. The first was in the form of Eq. (3) with τ_r equal to τ_c. The second term, referred to now as the Callaway correction term, results from the different effects of *N* and *U* processes described by Eq. (5), and was assumed negligible. Scattering from imperfections and at the crystal boundaries was included. The fitted function gives reasonable values below and around the maximum in the thermal conductivity ($\simeq 12$ K), but not at higher temperatures.[17]

Holland[17] extended the Callaway model by separating the contributions of longitudinal and transverse phonons, including an approximate phonon dispersion relation, and using different forms of the relaxation times. The Callaway correction term was neglected, and the *N* processes were treated as an additional, but not special, scattering mechanism in the formulation of the total relaxation time. For germanium, the high-temperature predictions are in better agreement with the experimental data than those from the Callaway model. The Holland model has since been used to investigate many other materials, and refined to account for more realistic phonon dispersion,[18] the effect of the Callaway correction term,[19] and additional phonon scattering mechanisms[15] (e.g., four-phonon processes and dislocations). The added complexity leads to more fitting parameters. One could argue that better agreement with experimental data is a result of these additional fitting parameters, and not an improvement of the actual physical model.

More refined BTE-SMRT models have been developed,[1] and more general solutions to the BTE based on iterative methods also exist.[20,21] However, as a result of the complexity of the required calculations, investigators continue to use the models of Callaway and Holland with only slight modifications, mainly due to the ease with which they can be implemented and their general success (albeit with the use of multiple fitting parameters).

B. Green-Kubo method: statistical mechanics approach

In a MD simulation, the classical position and momentum space trajectories of a system of particles are determined using interatomic forces (which are calculated from an appropriate potential-energy function), Newton's second law, and the kinematic equations of motion. The net flow of heat in such a system, given by the heat current vector **q**, fluctuates about zero at equilibrium. In the GK method, the thermal conductivity is related to how long it takes for these fluctuations to dissipate, and is given by[3]

$$k = \frac{1}{k_B V T^2} \int_0^\infty \frac{\langle \mathbf{q}(t) \cdot \mathbf{q}(0) \rangle}{3} dt, \tag{7}$$

where k_B is the Boltzmann constant, V is the volume of the simulation cell, and $\langle \mathbf{q}(t) \cdot \mathbf{q}(0) \rangle$ is the heat current autocorrelation function (HCACF). The heat current vector for a pair potential is given by[3]

$$\mathbf{q} = \frac{d}{dt} \sum_i E_i \mathbf{r}_i = \sum_i E_i \mathbf{v}_i + \frac{1}{2} \sum_{i,j} (\mathbf{F}_{ij} \cdot \mathbf{v}_i) \mathbf{r}_{ij}, \tag{8}$$

where E_i, $\mathbf{r}_i$, and $\mathbf{v}_i$ are the energy, position vector, and velocity vector of particle *i*, respectively, and $\mathbf{r}_{ij}$ and $\mathbf{F}_{ij}$ are the interparticle separation vector and force vector between particles *i* and *j*, respectively. The GK method has been used in MD simulations of dielectric materials such as amorphous silicon,[4] LJ argon,[5,9] diamond,[7] β-silicon carbide,[6] silicon,[8] and silica based crystals.[10]

It has been shown[7,9] that the thermal conductivity of a crystal with a monatomic unit cell can be decomposed into contributions from short and long length scale interactions by fitting the HCACF to a function of the form

$$\frac{\langle \mathbf{q}(t) \cdot \mathbf{q}(0) \rangle}{3} \equiv A_{ac,sh} \exp(-t/\tau_{ac,sh}) + A_{ac,lg} \exp(-t/\tau_{ac,lg}). \tag{9}$$

Here, the subscripts ac, sh, and lg refer to acoustic phonons, short range, and long range, respectively. The A terms are constants, and the τ terms are time constants. Using Eqs. (7) and (9), we have

$$k = \frac{1}{k_B V T^2} (A_{ac,sh} \tau_{ac,sh} + A_{ac,lg} \tau_{ac,lg}) \equiv k_{ac,sh} + k_{ac,lg}. \tag{10}$$

The short-range component is associated with phonons with a mean free path equal to one half of their wavelength (the limiting physical value[22–24]), while the long-range component describes phonons with longer mean free paths. The short-range component and its associated time constant are independent of temperature. The long-range component is temperature dependent. It accounts for the majority of the thermal conductivity, except at high temperatures, where it is diminished due to the increased anharmonicity in the atomic interactions.

III. MOLECULAR-DYNAMICS SIMULATIONS

The fcc LJ crystal is studied. The plane formed by the [100] and [010] axes is shown in Fig. 2. In the figure, a is the side length of the conventional unit cell (which contains four atoms) and L is the side length of the simulation cell (which is taken to be cubic). This leads to $\eta = L/a$ unit cells in each of the [100], [010], and [001] directions, and $N = 4\eta^3$ total atoms. Values of η of four, five, and six are used, which correspond to 256, 500, and 864 total atoms, respectively. Simulation cells of different sizes are required to obtain the necessary resolution of the wave vectors in the first Brillouin

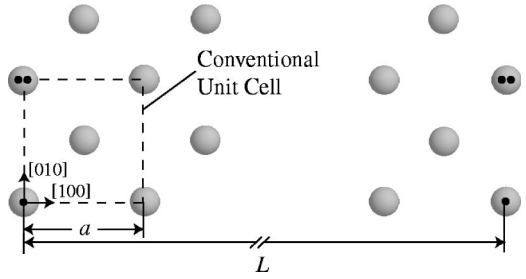

FIG. 2. A plane in the fcc crystal. The atoms with black dots are equivalent through the use of periodic boundary conditions.

zone in the BTE-SMRT approach. We define a dimensionless wave vector $\boldsymbol{\kappa}^*$ as

$$\boldsymbol{\kappa}^* = \frac{\boldsymbol{\kappa}}{2\pi/a}, \tag{11}$$

such that $\boldsymbol{\kappa}^*$ will vary between zero and one in the [100] direction in the first Brillouin zone.

In an LJ system, the potential energy, U_{ij}, between atoms i and j $(i \neq j)$ is given by[25]

$$U_{ij}(r_{ij}) = 4\epsilon_{\mathrm{LJ}}\left[\left(\frac{\sigma_{\mathrm{LJ}}}{r_{ij}}\right)^{12} - \left(\frac{\sigma_{\mathrm{LJ}}}{r_{ij}}\right)^{6}\right]. \tag{12}$$

The depth of the potential energy well is ϵ_{LJ}, and corresponds to an equilibrium particle separation of $2^{1/6}\sigma_{\mathrm{LJ}}$. The LJ potential describes the noble elements well. Argon, for which σ_{LJ} and ϵ_{LJ} have values of 3.40×10^{-10} m and 1.67×10^{-21} J, respectively,[25] is chosen for the current investigation. The use of a simple system allows for fast simulation runs and the elucidation of results that may be difficult to resolve in more complex materials.

The simulations are run in the *NVE* (constant mass, volume, and energy) ensemble at zero pressure with a time step of 4.285 fs, and periodic boundary conditions are imposed in all directions. Temperatures of 20 K, 35 K, 50 K, 65 K, and 80 K are considered. The melting temperature of the MD simulation cell is around 87 K. The unit-cell parameters are given in Table I. The details of the MD procedures have been described elsewhere.[9] The only significant modifications made here are that the potential cutoff is fixed at $2.5\sigma_{\mathrm{LJ}}$ and no correction is made to the pressure calculation. These changes ensure that the atomic spacing is the same in the different sized simulation cells.

Due to their classical nature, MD simulations cannot explicitly take quantum effects into account. The MD approach is thus not suitable near and below the maximum in the thermal conductivity [observed experimentally in crystals around one-tenth of the Debye temperature[26], and for argon at a temperature of 6 K (Ref. 27)], where quantum effects on the phonon mode populations are important. The thermal conductivity in this region is also strongly affected by impurities and boundary effects, which are not considered here. As such, an MD simulation of a perfect crystal with periodic boundary conditions will lead to an infinite thermal conductivity at zero temperature, as opposed to the experimental value, which goes to zero. Although temperature and thermal conductivity scaling factors have been suggested that include quantum effects,[4,6,8] these are not used here, as quantum effects are not expected to be significant for argon in the temperature range considered.[25]

IV. GREEN-KUBO THERMAL CONDUCTIVITY PREDICTION

The thermal conductivities predicted using the GK method are given in Table I. Each value corresponds to the average of five independent simulations. Also included is the decomposition of the thermal conductivity into the short-range and long-range components, and the associated time

TABLE I. Simulation cell parameters and GK thermal conductivity predictions. The specific heat is given per degree of freedom.

T (K)	a (Å)	η	c_v/k_{B}	k_{GK} (W/m-K)	$k_{ac,sh}$ (W/m-K)	$k_{ac,lg}$ (W/m-K)	$\tau_{ac,sh}$ (ps)	$\tau_{ac,lg}$ (ps)
0	5.269		1					
20	5.315	4	0.976	1.216	0.080	1.137	0.289	8.161
		5		1.217	0.074	1.143	0.275	7.776
		6		1.218	0.069	1.149	0.263	7.617
35	5.355	4	0.957	0.580	0.090	0.491	0.290	4.438
		5		0.587	0.086	0.501	0.281	4.183
		6		0.593	0.088	0.505	0.286	4.279
50	5.401	4	0.944	0.323	0.100	0.223	0.289	2.669
		5	0.941	0.348	0.091	0.257	0.271	2.518
		6	0.942	0.336	0.089	0.246	0.266	2.400
65	5.455	4	0.930	0.219	0.095	0.124	0.261	1.560
		5		0.223	0.093	0.130	0.254	1.601
		6		0.236	0.098	0.138	0.264	1.826
80	5.527	4	0.924	0.162	0.082	0.080	0.225	0.894
		5		0.164	0.084	0.080	0.227	0.919
		6		0.177	0.099	0.078	0.247	1.313

constants [defined in Eqs. (9) and (10)].

The thermal conductivity predictions are lower than our previously reported data,[9] due to the smaller lattice spacing that results from the smaller potential cutoff and removal of the pressure correction. There is no size effect (the thermal-conductivity predictions fall within at most $\pm 5\%$ of the mean value at a given temperature), consistent with the result of Kaburaki *et al.*[5] for LJ systems with greater than 256 atoms ($\eta=4$). There is more variation in the components of the thermal-conductivity decomposition and associated time constants than in the total thermal conductivity, which is due to the nature of the fit of Eq. (9). While the total value of the resulting integral is consistent, there is some ''exchange'' between the two components where the dominant behavior changes from $\tau_{ac,sh}$ to $\tau_{ac,lg}$. This effect is particularly evident at the higher temperatures considered, where $\tau_{ac,sh} \sim \tau_{ac,lg}$.

The experimental values for the thermal conductivity of argon at the temperatures considered are 1.36 W/m-K (20 K), 0.65 W/m-K (35 K), 0.46 W/m-K (50 K), 0.35 W/m-K (65 K), and 0.30 W/m-K (80 K). (Ref. 28). In general, differences between predictions from MD simulations and experimental data can be attributed to the approximate nature of the interatomic potential, size effects, and the simulation procedures. By using a cutoff radius around $4\sigma_{\mathrm{LJ}}$, we note that good agreement can be found with the experimental thermal conductivity data for argon. In this investigation, we are concerned with checking the internal consistency between the GK and BTE-SMRT approaches, and as such, use the standard $2.5\sigma_{\mathrm{LJ}}$ cutoff.

V. BOLTZMANN TRANSPORT EQUATION FORMULATION

To use Eq. (3) to predict the thermal conductivity, c_v, τ_r, v_g, v_p, and the upper limits of the integrals must be specified.

A. Specific heat

The specific heat is defined thermodynamically as the rate of change of the total system energy (kinetic and potential) as a function of temperature at constant volume.[25] Such a calculation can be explicitly performed using the results of the MD simulations. The predicted specific heats are plotted in Fig. 3 and given in Table I for the $\eta=4$ simulation cells. The values given correspond to the specific heat per degree of freedom, as required by Eq. (3), and no frequency or polarization dependence is taken into account. The calculation is performed by varying the temperature in 0.1 K increments over a ± 0.2 K range around the temperature of interest. Five simulations are performed at each of the five increments, with energy data averaged over 3×10^5 time steps. The resulting 25 data points are fit with a linear function, whose slope is the specific heat. At a temperature of 50 K, the specific heat has been predicted for each of the simulation cell sizes (given in Table I), and no size dependence is evident. While the spread of the energy data in these calculations increases with increasing temperature (the R^2 value of the fit at a temperature of 20 K is 0.9999, while that at a temperature of 80 K is 0.9774), the consistency in the predicted specific heats suggests that any error present is minimal.

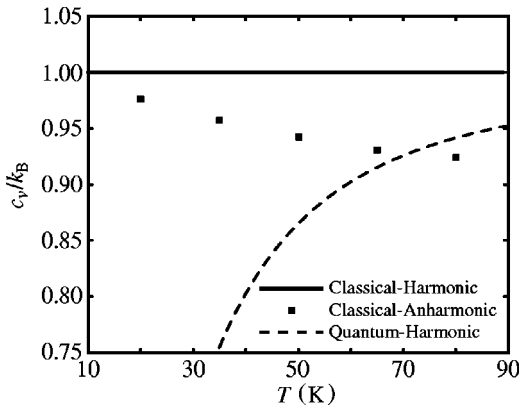

FIG. 3. The classical-anharmonic specific heat per degree of freedom predicted from the MD simulations, and the classical-harmonic and quantum-harmonic curves (all scaled by k_{B}).

The specific heat predicted from the MD simulations is a classical-anharmonic value. Also shown in Fig. 3 are the classical-harmonic and the quantum-harmonic specific heats. The classical-harmonic value k_{B} is based on an assumption of equipartition of kinetic and potential energy between normal modes. The equipartition assumption is always valid for the kinetic energy (i.e., it contributes 0.5 k_{B} to c_v). However, for the potential energy, it is only true under the harmonic approximation, which itself is only valid at zero temperature. The deviations of the classical-anharmonic results from the classical-harmonic model are significant. The quantum-harmonic specific heat is based on the zero-temperature phonon density of states (as calculated from the MD simulations) and is given by[29]

$$c_{v,quant\text{-}harm}=k_{\mathrm{B}}\sum_i \frac{x_i^2\exp(x_i)}{[\exp(x_i)-1]^2}, \tag{13}$$

where x is $\hbar\omega/k_{\mathrm{B}}T$, $\hbar$ is the Planck constant divided by 2π, and the summation is over the normal modes of the system. As expected, the classical and harmonic specific heats are significantly different at low temperatures, where quantum effects are important. Prediction of the quantum-anharmonic specific heat (as would be measured experimentally) would require taking into account the temperature dependence and coupling of the normal modes, and the results would be expected to converge with the classical-anharmonic value at high temperatures (i.e., on the order of the Debye temperature).

B. Phonon relaxation time

For the case of a monatomic unit cell, in a simulation cell with N atoms there are N points in the first Brillouin zone. Each point has one longitudinal and two transverse phonon modes associated with it. This leads to the $3N$ normal modes. By assuming an isotropic phonon dispersion, a

smaller subset can be considered in the thermal conductivity calculation. Here, the [100] direction is chosen, in which there will be η allowed modes. This does not include the zero-frequency mode, which corresponds to a rigid translation of the simulation cell, and does not contribute to thermal transport. To obtain a sufficient number of points within the first Brillouin zone to form a continuous τ_r function, different sized simulation cells must be considered. These have been described in Sec. III.

Ladd *et al.*[11] present a method in which the relaxation time of the ith mode $\tau_{i,r}$ is found using the time history of the mode potential energy $E_{i,p}$. This method is modified here by considering the total energy (potential and kinetic) of each mode, $E_{i,t}$.

The normal modes of a system, $S_i(\boldsymbol{\kappa}, \nu)$, where ν corresponds to the mode polarization (L or T) described by a vector $\mathbf{e}_i(\boldsymbol{\kappa}, \nu)$, can be expressed as a sum over the positions of the atoms in the system as

$$S_i(\boldsymbol{\kappa}, \nu) = N^{-1/2} \sum_j M_j^{1/2} \exp(-i\boldsymbol{\kappa} \cdot \mathbf{r}_{j,o}) \mathbf{e}_i^*(\boldsymbol{\kappa}, \nu) \cdot \mathbf{u}_j . \tag{14}$$

Here, M is the mass of an atom, * denotes the complex conjugate, $\mathbf{r}_{j,o}$ is the equilibrium position of atom j, and $\mathbf{u}_j$ is the relative displacement of atom j from its equilibrium position (i.e., $\mathbf{r}_j - \mathbf{r}_{j,o}$).

Under the harmonic approximation, the total energy of each mode of a classical system is given by

$$E_{i,t} = \frac{\omega_i^2 S_i^* S_i}{2} + \frac{\dot{S}_i^* \dot{S}_i}{2}, \tag{15}$$

where the first term corresponds to the potential energy and the second term to the kinetic energy. The temporal decay of the autocorrelation of $E_{i,t}$ is related to the relaxation time of that mode. The resulting curve for the transverse polarization at $\kappa^* = 0.5$ for the $\eta = 4$ simulation cell at a temperature of 50 K is shown in Fig. 4. The required ensemble average is realized by averaging the autocorrelation functions (10^4 time steps long, based on 2×10^5 time steps of data) over the [100], [010], and [001] directions over five independent simulations. This leads to 15 data sets for the longitudinal polarization and 30 data sets for the transverse polarization. The relaxation time is obtained by fitting the data with an exponential decay. Based on this formulation, the calculated time constant must be multiplied by two to get the relaxation time to be used in the BTE (this will be explained in Sec. VI B). All of the modes considered show a general behavior consistent with a single relaxation time. The only exceptions are the longitudinal modes below a κ^* value of 0.5, where a secondary decay is evident in the very early stages of the overall decay. In these cases, this portion of the autocorrelation is neglected when fitting the exponential. Alternatively, one could calculate the integral of the autocorrelation and from that deduce an effective relaxation time.[11] Due to the short extent of the observed deviation from a SMRT, and the subsequent fitting of a continuous function to the discrete relaxation times, the difference between this approach and that which has been adopted is negligible.

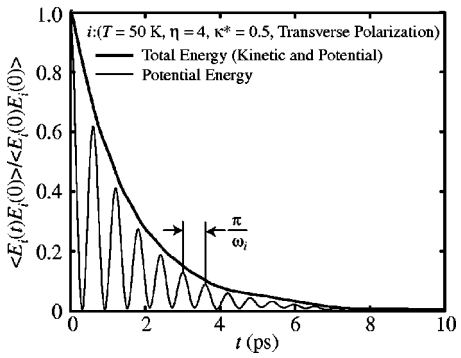

FIG. 4. Autocorrelation curves for the relaxation time and anharmonic phonon dispersion calculation methods. The data correspond to deviations from the mean energy values, and have been normalized against the zero time value of the autocorrelations. Shown are the total-mode energy (used in the relaxation time calculation) and the potential energy (used to obtain the anharmonic phonon dispersion). The frequency of the oscillations in the potential-energy curve is double that of the phonon mode in question because of the squaring operations in Eq. (15).

An indication of the error in the predicted relaxation times can be obtained by finding $\tau_{i,r}$ for each of the data sets before averaging the autocorrelation functions, and looking at the resulting spread. The mean values and standard deviations corresponding to the $\eta = 4$ simulation cell at a temperature of 50 K are given in Table II. The standard deviation is between 6% and 19% of the mean value for the longitudinal direction, and between 12% and 22% of the mean value for the transverse direction. These values are typical of those found for the other temperatures. Much of this uncertainty is eliminated when the relaxation times are fit with continuous functions. This is described next.

Having obtained a set of discrete $\tau_{i,r}$ values for a given temperature and polarization, a continuous function, τ_r, can now be constructed. The discrete and continuous results at a temperature of 50 K are plotted as $1/\tau_{i,r}$ (or $1/\tau_r$) vs ω [after Eq. (6)] in Fig. 5(a).

To be physically meaningful, the mean free path, Λ, of a phonon should be longer than one half of its wavelength, λ.[24,22,23] Noting that $\Lambda = v_g \tau_r$, $\lambda = 2\pi/\kappa$, and using the definition of v_p, this limit can alternatively be stated as

TABLE II. Mean values and spread of the discrete relaxation times at a temperature of 50 K for the $\eta = 4$ simulation cell. The calculations are based on finding the relaxation times before averaging the autocorrelation functions.

κ^*	$(\overline{\tau_{i,r}})_L$ (ps)	$(\sigma_{i,r})_L$ (ps)	$(\overline{\tau_{i,r}})_T$ (ps)	$(\sigma_{i,r})_T$ (ps)
0.25	7.50	1.42	6.31	0.88
0.50	3.34	0.63	2.90	0.35
0.75	1.38	0.07	2.87	0.40
1.00	1.11	0.07	2.70	0.59

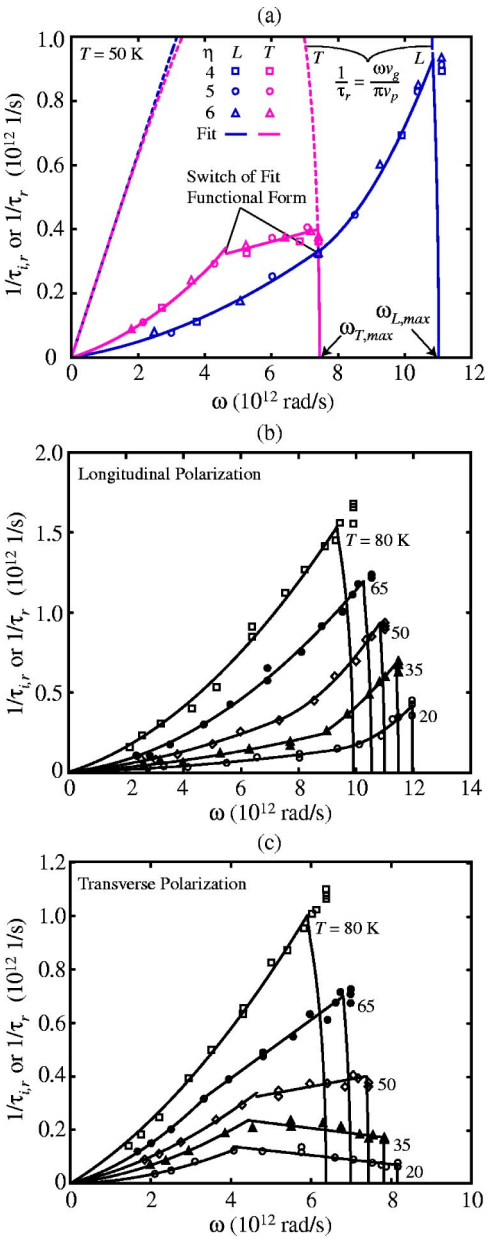

FIG. 5. (Color online) (a) Discrete relaxation times ($\tau_{i,r}$) and continuous curve fits (τ_r) at $T=50$ K. Also shown is the minimum physical value of the relaxation time, $\pi v_p/\omega v_g$. (b) Raw data and continuous relaxation time curve fits for the longitudinal polarization at all temperatures considered. (c) Raw data and continuous relaxation time curve fits for the transverse polarization at all temperatures considered.

$$\frac{1}{\tau_r} \leqslant \frac{\omega v_g}{\pi v_p}, \tag{16}$$

and is also shown in Fig. 5(a). At a temperature of 50 K, the phonons at the edge of the first Brillouin zone ($\kappa^*=1$) are outside of the allowed range for both polarizations. As the temperature increases, more of the phonon modes do not satisfy Eq. (16). At the highest temperature, 80 K, the transition occurs at κ^* values of 0.77 and 0.81 for the longitudinal and transverse polarizations, respectively.

The data for each polarization can be broken down into three distinct regions. The first two are fit with low-order polynomials. For the longitudinal polarization, the first region is fit with a second-order polynomial through the origin, and the second region with a second-order polynomial. For the transverse polarization, the first region is fit with a second-order polynomial through the origin, and the second region with a linear function. The resulting functions are also shown in Fig. 5(a) and are considered satisfactory fits to the MD data. As the temperature increases, the behavior in the two regions becomes similar. For both polarizations at a temperature of 80 K, and for the longitudinal polarization at a temperature of 65 K, a single second-order polynomial through the origin is used to fit the data. In the third region, the continuous relaxation time functions are taken up to the maximum frequency ($\omega_{L,max}$ or $\omega_{T,max}$) using Eq. (16).

The raw data and continuous relaxation time functions for all temperatures considered are shown in Figs. 5(b) and 5(c). The parts of the relaxation time curves are not forced to be continuous. For both the longitudinal and transverse polarizations, any resulting discontinuities are small, and are purely a numerical effect. The relaxation time functions do not contain the orders of magnitude discontinuities found in the Holland relaxation times for germanium, which result from the assumed forms of the relaxation times, and how the fitting parameters are determined.[30]

Theoretical calculations predict that in the κ^* range 0–0.2, the longitudinal and transverse curves should follow ω^2 and ω dependencies, respectively.[16,31] This is not found in the relaxation times predicted by the MD simulations. The second order fit found at the high temperatures is consistent with the high-temperature prediction of Srivastava.[1] Of particular note is the turning over of the low-temperature transverse curves at higher frequencies. In general, it is clear that the extension of the low-frequency behavior to the entire frequency range, as is sometimes done, is not generally suitable. The effect of such an assumption on the thermal conductivity prediction will be considered in Sec. VI C.

C. Phonon dispersion

The phonon dispersion relation for a solid describes the relationship between the phonon frequencies and their wavelengths. It can thus be used to predict the phonon phase and group velocities, and the upper integration limits, required for the evaluation of Eq. (3). In some BTE-SMRT investigations,[14,17,24] the dispersion has been either neglected or greatly simplified. The importance of accurately modeling the dispersion has recently been investigated for germanium.[30] The assumption of no dispersion is found to contribute to nonphysical discontinuities in the relaxation times, which are masked in the final calculation of the thermal conductivity with the use of fitting parameters. By more accurately modeling the dispersion, the size of these discontinuities can be reduced (although they are not eliminated due to the relaxation time models used).

The zero-temperature phonon dispersion is harmonic, and can be determined exactly at any wave vector using the MD equilibrium atomic positions and the interatomic potential. A

continuous dispersion relation can thus be obtained. Deviations from this calculation at finite temperature are a result of two effects.[2] Based on the higher-order terms in the expansion of the potential energy about its minimum, a solid will either expand (as seen here), or contract (e.g., some zeolites), as the temperature increases. An expansion will cause the phonon frequencies to decrease. Recalculating the dispersion harmonically with the new lattice constant is known as the quasiharmonic approximation.[2] The second effect is a result of anharmonicities in the atomic interactions, which become increasingly important as the temperature is increased. The exact modeling of this effect is difficult. To account for the anharmonic effects, the autocorrelation data for the mode potential energy are used to calculate the frequencies of the discrete modes present in the MD simulations. This is shown in Fig. 4. While the total-energy autocorrelation shows a monotonic decay, that for the potential-energy oscillates. This is an indication of the total mode energy having both potential -and kinetic-energy components. An estimate of the anharmonic frequency is obtained by averaging over all non-negligible oscillations in the autocorrelation. This generates a set of discrete anharmonic frequency data. These values are then compared to the associated quasiharmonic frequencies, and a second-order polynomial scaling function is constructed. This function is then applied to the continuous quasiharmonic data to obtain the full anharmonic dispersion. The excellent quality of the mapping from the quasiharmonic data to the anharmonic data (the R^2 values of the scaling functions are ~ 0.999) suggests that minimal error is introduced through this procedure.

The frequencies used for the horizontal axes of Figs. 5(a), 5(b), and 5(c) are based on the anharmonic dispersion. We note, however, that the frequencies used in the phonon energy calculations [Eqs. (14) and (15)] must be those corresponding to the quasiharmonic dispersion. This is a result of the phonon dynamics being based on a harmonic theory, while the BTE expression for the thermal conductivity is not. The need to use the quasiharmonic frequencies in the phonon energy calculation has been justified by calculating the total, average phonon potential energy and comparing the result to that directly calculated with the LJ potential. Using the quasiharmonic frequencies results in an energy that matches the magnitude and temperature trend of the exact calculation to within 5% over the entire temperature range considered. The anharmonic results diverge from the exact calculation, and are 36% larger at the highest temperature.

The phonon dispersion for the [100] direction is shown in Fig. 6(a) for the zero-temperature simulation cell, and for the quasiharmonic and anharmonic predictions at a temperature of 50 K. The resulting v_g/v_p^2 functions, which are required in Eq. (3), are shown in Fig. 6(b). The effect of the unit-cell size is significant, and increases with increasing temperature. The anharmonic effects are significant for the longitudinal polarization at all temperatures, and increase with increasing temperature. For the transverse polarization, the deviations from the quasiharmonic values are only found to be significant at a temperature of 80 K. To our knowledge, the temperature dependence of the dispersion has not previously been considered in the SMRT formulation. Typically, one set

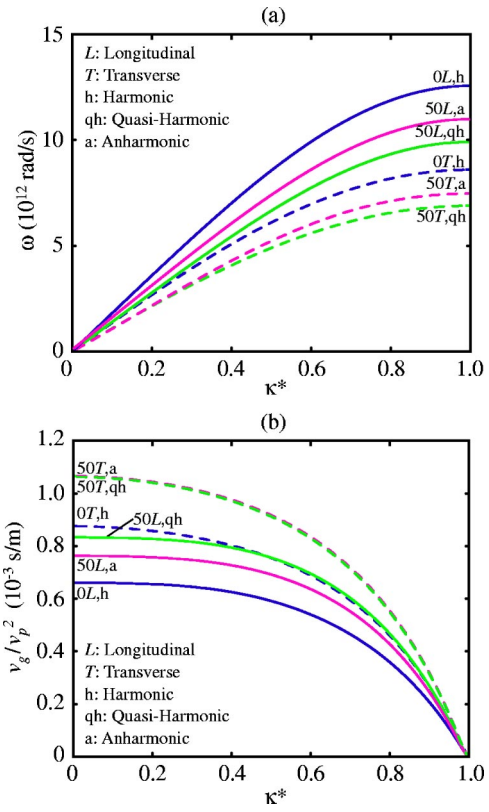

FIG. 6. (Color online) (a) Phonon dispersion in the [100] direction. (b) Variation of v_g/v_p^2 for the dispersion relations of part (a). The curves are identified by the temperature in Kelvin, the polarization, and the nature of the calculation (h=harmonic, qh =quasiharmonic, a=anharmonic). The (50*T*,a) and (50*T*,qh) curves are indistinguishable in (b).

of low-temperature data (which is more readily obtained experimentally than high temperature data) is applied over the entire temperature range of interest. As seen in Figs. 6(a) and 6(b), such assumption is rather questionable.

VI. BOLTZMANN TRANSPORT EQUATION THERMAL-CONDUCTIVITY PREDICTION

Having specified the specific heat, phonon velocities, and phonon relaxation times, the thermal conductivity can be predicted using Eq. (3). As the LJ fcc crystal has a monatomic unit cell, there are only acoustic phonon modes present, and the assumption of neglecting optical phonon modes is not relevant. The results are given in Table III and shown in Figs. 7(a) and 7(b). Included in Table III are the total values of the thermal conductivity and their decomposition into longitudinal and transverse components, along with the mean GK values, calculated from Table I.

A. Validation of the BTE-SMRT approach

In order to compare the GK and BTE-SMRT predictions, the nature of each method and the associated uncertainties must be considered.

In the GK method, the thermal conductivity is predicted without making any *a priori* assumptions about the nature of

TABLE III. BTE-SMRT and GK thermal conductivity predictions. $k_{BTE}=k_L+2k_T$.

T (K)	k_{GK} (W/m-K)	k_{BTE} (W/m-K)	k_L (W/m-K)	k_T (W/m-K)
20	1.217	1.440	0.751	0.345
35	0.587	0.675	0.368	0.154
50	0.335	0.373	0.198	0.087
65	0.226	0.220	0.112	0.054
80	0.167	0.134	0.066	0.034

the thermal transport. As such, we take the prediction of this method to be the ''exact'' MD value that the BTE-SMRT method should be compared to. As discussed in Sec. IV and Ref. 9, the uncertainty in the GK values is $\pm 5\%$.

The complicated nature of the BTE-SMRT formulation makes it difficult to assign a uncertainty to the results without making multiple predictions at a given temperature. Due to the need to use different simulation cell sizes, the BTE-SMRT approach is significantly more computationally demanding than the GK approach, making additional predictions costly. A second set of thermal conductivity predictions at temperatures of 20 K, 50 K, and 80 K resulted in values of 1.444 W/m-K, 0.369 W/m-K, and 0.133 W/m-K, respectively. The good agreement with the thermal conductivities given in Table III indicates that the uncertainty in the BTE-SMRT thermal conductivity predictions is on the order of

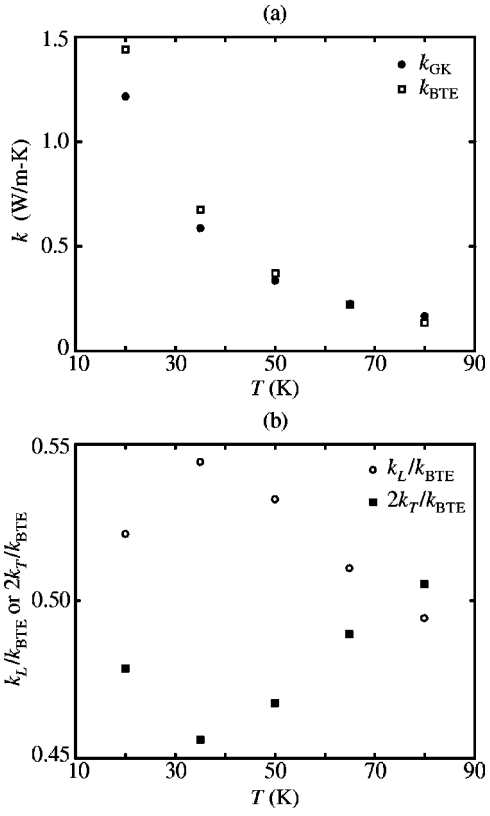

FIG. 7. (a) Thermal conductivities predicted by the GK and BTE-SMRT methods. (b) The relative contributions of the longitudinal and transverse polarizations to k_{BTE}.

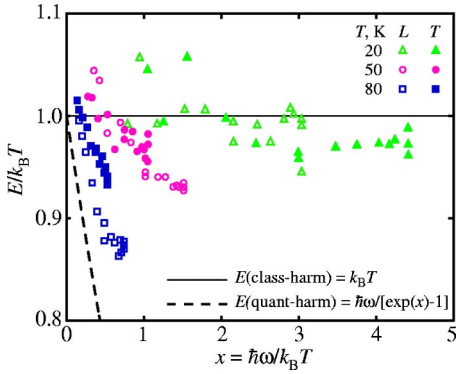

FIG. 8. (Color online) Average phonon mode energies scaled by k_BT at temperatures of 20 K, 50 K, and 80 K. Also shown are the quantum-harmonic and classical-harmonic energies.

that for the GK values (i.e., 5%). The observed repeatability is in large part a result of the many independent simulations used to provide data for a given condition. A complete sampling of the MD phase space is crucial for obtaining good statistics with minimal noise.

In the BTE-SMRT approach, two important points must be considered. First, the phonon dispersion has been assumed isotropic. The volume of the associated first Brillouin zone, which is spherical, is $32\pi^4/3a^3$. The volume of the real first Brillouin zone is $32\pi^3/a^3$, which means that the volume considered in the integral is $\pi/3\simeq 1.05$ times larger than the real volume. The isotropic assumption also affects the phonon relaxation times and velocities, and the results indicate that these factors lead to an overprediction of the thermal conductivity. This effect is consistent with the predictions of an iterative solution method for the BTE.[20]

Second, the BTE-SMRT formulation has a harmonic basis. Even though anharmonicities have been taken into account in the phonon dispersion, the expression for $E_{i,t}$ [Eq. (15)] assumes a harmonic system. As the temperature is increased, the validity of this assumption worsens, and leads to an underprediction of the thermal conductivity at the higher temperatures (i.e., the anharmonic effect dominates over the isotropic effect). The deviation from the harmonic theory is seen in the specific-heat data (Table I and Fig. 3), and by plotting the average phonon energies (scaled by the classical expectation value, k_BT), as shown in Fig. 8. Also shown in Fig. 8 is the quantum-harmonic phonon energy. At the low temperatures, the agreement between the MD data and the classical prediction is reasonable, but steadily worsens as the temperature increases. The existence of modes with energy greater than the classical value can be attributed to the harmonic nature of the energy calculation.

Based on the above discussion, the agreement between the two independent predictions of the thermal conductivity is considered satisfactory. Thus, for what we believe to be the first time, we have established the quantitative validity of the BTE-SMRT approach. The BTE-SMRT formulation could be improved by removing the isotropic assumption and considering the frequency dependence of the specific heat. However, both of these steps would result in more time intensive calculations, for which the resources may not always be available.

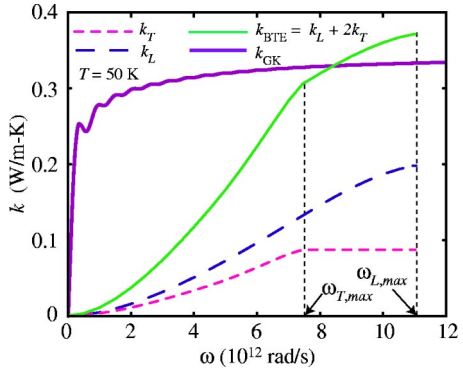

FIG. 9. (Color online) Cumulative frequency dependence of the thermal conductivity at a temperature of 50 K.

B. Investigation of GK and BTE-SMRT formulations

To compare the GK and BTE-SMRT methods, the cumulative frequency dependencies of the thermal conductivities predicted by Eqs. (3) and (7) can be considered.[9] This is shown in Fig. 9. The GK curve corresponds to the $\eta=6$ simulation cell for a temperature of 50 K. The oscillations are a function of the periodic boundary conditions. The majority of the GK thermal conductivity is accounted for by a frequency range much smaller than that of the phonon spectrum ($0<\omega<\omega_{L,max}$). To understand this behavior, the difference between the phonon frequency and the frequency associated with the phonon relaxation time must be distinguished. This is seen by expressing the normal modes as[11]

$$S_i = S_{i,o}\exp[-i(\omega_i + i\Gamma_i)t], \tag{17}$$

where $S_{i,o}$ is the mean value and Γ_i is the line width, equal to $1/(2\tau_{i,r})$ (this is the factor of two that comes into the relaxation time calculation in Sec. V B). In the BTE formulation, Eq. (3), the integration is over the phonon frequency ω_i. In the GK formulation, Eq. (7), the integration is over the frequency corresponding to the phonon lifetime $2\Gamma_i$ which will be many times the period of oscillation $2\pi/\omega_i$.

The effect of temperature on the BTE-SMRT prediction can be assessed by plotting the cumulative wave-number dependence of the thermal conductivity. This is shown in Fig. 10 for all the temperatures considered, with the thermal conductivity normalized against the total value. Note that there is no apparent temperature effect. A given phonon mode contributes equally to the thermal conductivity, independent of the temperature. As well, the weighting of the contribution of the modes to the total thermal conductivity is approximately uniform. Both of these findings are contrary to the common notion that as the temperature decreases, long wavelength (low wave number) modes become increasingly important. In analytical BTE-SMRT calculations, such a finding may have come about due to the assumed piecewise forms of the phonon relaxation times. We note that this behavior may also be partially a result of the classical nature of the simulations, where all modes are excited approximately equally (see Fig. 8). This is not true of a quantum system at low temperature.

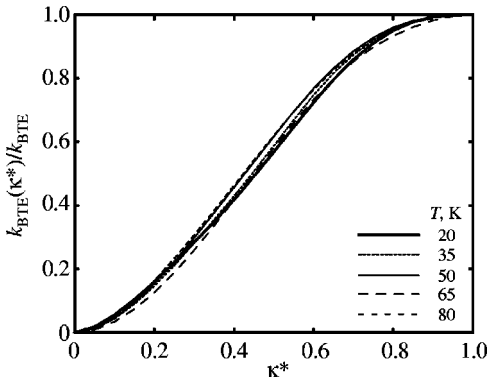

FIG. 10. Cumulative wave-number dependence of the BTE-SMRT thermal conductivity at all temperatures considered. The thermal conductivity is normalized against the total value.

TABLE IV. BTE-SMRT thermal conductivity predictions at a temperature of 50 K under simplifying assumptions. $k_{BTE}=k_L+2k_T$. (a) $T=50$ K, no dispersion, (b) $T=0$ K dispersion, (c) $T=50$ K quasiharmonic dispersion, (d) low-frequency relaxation time behavior extended to entire frequency range, and (e) single relaxation time ($\tau_{ac,lg}$). Under the full model, $k_{BTE}=0.373$ W/m-K, $k_L=0.198$ W/m-K, and $k_T=0.087$ W/m-K.

	k_{BTE} (W/m-K)	k_L (W/m-K)	k_T (W/m-K)
(a)	0.482	0.239	0.122
(b)	0.383	0.187	0.098
(c)	0.332	0.190	0.071
(d)	0.357	0.208	0.074
(e)	0.264	0.144	0.060

It is also interesting to note that the relative contributions of the longitudinal and transverse polarizations change by only a small amount over the large temperature range considered, as shown in Fig. 7(b) ($k_L/k_{BTE}\sim0.5$ and $k_T/k_{BTE}\sim0.25$). This is in contrast to predictions made for germanium, where, albeit with a different crystal structure, the transverse phonon modes are predicted to account for the majority of the thermal conductivity at high temperatures.[30]

C. Simplifying assumptions in the BTE-SMRT approach

To assess the importance of the detail used in the modeling of the terms in Eq. (3), a number of approximations are investigated at a temperature of 50 K. The results are summarized in Table IV for the following cases: (a) assuming no dispersion [i.e. $v_g=v_p$, so that $v_g/v_p^2=1/v_g$, with the value taken as the $\kappa^*=0$ intercept for the ($50L$,a) and ($50T$,a) curves of Fig. 6(b)], (b) using the zero-temperature dispersion relation, (c) using the quasiharmonic dispersion, (d) extending the low-frequency relaxation time behavior over the entire frequency range, and (e) using a single time constant, taken as $\tau_{ac,lg}$ from the thermal conductivity decomposition of Eq. (10).

Assuming no phonon dispersion results in an overprediction of thermal conductivity. As is evident from Fig. 6(b), taking v_g/v_p^2 to be constant and equal to the $\kappa^*=0$ value will overemphasize the contributions of higher frequencies. Using the zero-temperature dispersion results in a similar value as the full model. This is due to two counteracting

effects: the extension of the integration limits in Eq. (3), which will raise the thermal conductivity, and the resulting lower values of v_g/v_p^2 [as seen in Fig. 6(b)], which will lower the thermal conductivity. Use of the quasiharmonic dispersion results in an underprediction of the thermal conductivity. Using the low-frequency relaxation time behavior extended over the entire frequency range results in an underprediction of the thermal conductivity. This can be largely attributed to the high-frequency behavior of the transverse polarization relaxation time curve, not captured in the trend of the low-frequency behavior. This discrepancy increases as the temperature is decreased [see Fig. 5(c)]. Using $\tau_{ac,lg}$ (2.53 ps) as a single relaxation time underpredicts the thermal conductivity. This is because it results in a near elimination of the low-frequency contributions. These findings indicate that taking the temperature and frequency dependencies of the relaxation times and phonon dispersion into account is crucial for obtaining a good and physical prediction of the thermal conductivity.

VII. SUMMARY AND CONCLUSION

The quantitative validity of the BTE-SMRT approach for predicting the phonon thermal conductivity has been validated for the LJ argon fcc crystal by using MD simulations to provide the necessary input, and then comparing the results to the predictions of the GK method. This approach eliminates the need for experimental fitting parameters. The success of the predictions is strongly dependent on the complete modeling of the temperature and frequency dependencies of the phonon dispersion and relaxation times. Assumptions commonly made in the BTE-SMRT approach (e.g., extension of the low-frequency behavior of the relaxation times over the entire frequency range, no dispersion, and/or temperature independent dispersion) can lead to poor predictions, which suggests that the previous success of these models (e.g., the Callaway-Holland approach) was strongly dependent on fitting the results to experimental data. The approach presented here is limited by the assumption of an isotropic medium and the harmonic nature of the relaxation time model. However, the error introduced by these factors is small compared to the gain associated with the elimination of fitting parameters. The methods described can be extended to other dielectric crystals, including those with multiatom unit cells (where optical phonons will be present).

Two sets of time constants have been introduced: those associated with the relaxation of particular phonon modes (τ_r), and those associated with the thermal-conductivity decomposition ($\tau_{ac,sh}$ and $\tau_{ac,lg}$). Both sets of relaxation times can be used to predict the thermal conductivity, and reasonable agreement in the results has been found. This agreement suggests that there is a link between these time constants, likely of the form

$$\tau_i = \sum_j \int_0^{\omega_{j,max}} g_j(\omega)(\tau_r)_j d\omega, \quad i=(ac,sh),(ac,lg), \tag{18}$$

where the sum is over the phonon polarizations, and $g_j(\omega)$ is a weighting function. The form of the weighting function may be related to the phonon distribution function and the nature of the three-phonon interactions.

The plots in Figs. 9 and 10 dispel a common misconception that the low-frequency/long-wavelength phonon modes dominate the thermal conductivity. In fact, long length scale behavior is important [the $k_{ac,lg}$ term in Eq. (10)], but it is the phonon mean free path, and not its wavelength, that is relevant. This is the important distinction seen when comparing the GK and BTE results in Fig. 9, as described by Eq. (17).

The development of relaxation time models is useful for thermal conductivity calculations as used, but will also be applicable to more general BTE calculations, including numerical solutions based on the phonon equation of radiation transfer[32] and the direct simulation Monte Carlo techniques.[33] Both of these approaches can be used to model larger system sizes (up to the micron level, typical of MEMS devices and not accessible with MD). In such calculations, simple relaxation time models have been used, and in some cases, a single relaxation time has been assumed to describe an entire system. The use of MD to generate continuous relaxation functions (without the need for experimental fitting parameters) will greatly add to the ability of such calculations to accurately model the underlying physics.

ACKNOWLEDGMENTS

This work has been supported by the U.S. Department of Energy, Office of Basic Energy Sciences under Grant No. DE-FG02-00ER45851, and the Horace H. Rackham School of Graduate Studies at the University of Michigan (AJHM).

*Electronic address: kaviany@umich.edu

[1] G. P. Srivastava, *The Physics of Phonons* (Adam Hilger, Bristol, 1990).

[2] M. T. Dove, *Introduction to Lattice Dynamics* (Cambridge University Press, Cambridge, 1993).

[3] D. A. McQuarrie, *Statistical Mechanics* (University Science Books, Sausalito, 2000).

[4] Y.H. Lee, R. Biswas, C.M. Soukoulis, C.Z. Wang, C.T. Chan, and K.M. Ho, Phys. Rev. B **43**, 6573 (1991).

[5] H. Kaburaki, J. Li, and S. Yip, in *Multiscale Modeling of Materials*, edited by T. Diaz de la Rubia, T. Kaxiras, V. Bulatov, N.M. Ghoniem, and R. Phillips, MRS Symposia Proceedings No. 538 (Materials Research Society, Pittsburgh, 1999), p. 503.

[6] J. Li, L. Porter, and S. Yip, J. Nucl. Mater. **255**, 139 (1998).

[7] J. Che, T. Cagin, W. Deng, and W. A. Goddard III, J. Chem. Phys. **113**, 6888 (2000).

[8] S. Volz and G. Chen, Phys. Rev. B **61**, 2651 (2000).

[9] A. J. H. McGaughey and M. Kaviany, Int. J. Heat Mass Transfer **47**, 1783 (2004).

[10] A. J. H. McGaughey and M. Kaviany, Int. J. Heat Mass Transfer **47**, 1799 (2004).

[11] A.J.C. Ladd, B. Moran, and W.G. Hoover, Phys. Rev. B **34**, 5058 (1986).

[12] C. Oligschleger and J.C. Schon, Phys. Rev. B **59**, 4125 (1999).

[13] K.C. Sood and M.K. Roy, J. Phys.: Condens. Matter **5**, 301 (1993).
[14] J. Callaway, Phys. Rev. **113**, 1046 (1959).
[15] M. Asen-Palmer, K. Bartkowski, E. Gmelin, M. Cardona, A.P. Zhernov, A.V. Inyushkin, A. Taldenkov, V. Ozhogin, K.M. Itoh, and E.E. Haller, Phys. Rev. B **56**, 9431 (1997).
[16] C. Herring, Phys. Rev. **95**, 954 (1954).
[17] M.G. Holland, Phys. Rev. **132**, 2461 (1963).
[18] M.D. Tiwari and B.K. Agrawal, Phys. Rev. B **4**, 3527 (1971).
[19] K.C. Sood and M.K. Roy, J. Phys.: Condens. Matter **5**, L245 (1993).
[20] M. Omini and A. Sparavigna, Phys. Rev. B **53**, 9064 (1996).
[21] A. Sparavigna, Phys. Rev. B **65**, 064305 (2002).
[22] D.G. Cahill and R.O. Pohl, Solid State Commun. **70**, 927 (1989).
[23] D.G. Cahill, S.K. Watson, and R.O. Pohl, Phys. Rev. B **46**, 6131 (1992).
[24] J.R. Olson, R.O. Pohl, J.W. Vandersande, A. Zoltan, T.R. Anthony, and W.F. Banholzer, Phys. Rev. B **47**, 14 850 (1993).
[25] N. W. Ashcroft and N. D. Mermin, *Solid State Physics* (Saunders College Publishing, Fort Worth, 1976).
[26] A. Majumdar, in *Microscale Energy Transport*, edited by C.-L. Tien, A. Majumdar, and F. M. Gerner (Taylor and Francis, Washington, 1998), p. 72.
[27] D.K. Christen and G.L. Pollack, Phys. Rev. B **12**, 3380 (1975).
[28] Y. Touloukian, *Thermophysical Properties of Matter* (Plenum, New York, 1970), Vol. 3.
[29] L. Porter, J. Li, and S. Yip, J. Nucl. Mater. **246**, 53 (1997).
[30] J. D. Chung, A. J. H. McGaughey, and M. Kaviany, J. Heat Transfer (to be published).
[31] J.E. Parrott, Proc. Phys. Soc. London **81**, 726 (1963).
[32] J.D. Chung and M. Kaviany, Int. J. Heat Mass Transfer **43**, 521 (2000).
[33] S. Mazumder and A. Majumdar, J. Heat Transfer **123**, 749 (2001).